Fuel 113 (2013) 787–797

Contents lists available at SciVerse ScienceDirect

Fuel

journal homepage: www.elsevier.com/locate/fuel

Trends in fireside corrosion damage to superheaters in air and oxy-firing of coal/biomass ☆

T. Hussain *, A.U. Syed, N.J. Simms

Centre for Energy & Resource Technology, Cranfield University, Bedfordshire MK43 0AL, UK

HIGHLIGHTS

- T92, 347HFG, HR3C and 625 have been tested in simulated air-fired and oxy-fired combustion gases at 600–750 °C.
- In both firing conditions characteristic "bell-shaped" curves of fireside corrosion damage was observed.
- The highest damage levels (peaks) were observed at 650 °C in air-fired conditions and 700 °C in oxy-fired conditions.
- The increase in peak corrosion damages in oxy-firing environment was due to the higher levels of SOx gases.
- Generally, the alloys had the following ranking (most to the least damage): T92 > 347HFG > HR3C > 625.

ARTICLE INFO

Article history:
Received 30 September 2012
Received in revised form 30 March 2013
Accepted 4 April 2013
Available online 23 April 2013

Keywords:
Biomass/coal co-firing
Oxy-firing
Air-firing
Coal-ash corrosion
Fireside corrosion

ABSTRACT

This paper compares the laboratory-based fireside corrosion tests on superheater/reheater materials in simulated air-firing combustion conditions with oxy-firing combustion conditions (with hot gas recycling before flue gas de-sulphurisation). The gaseous combustion environment was calculated based on a specific co-firing ratio of CCP with Daw Mill coal. The fireside corrosion tests were carried out using the "deposit recoat" test method to simulate the damage anticipated in specific environments. A synthetic deposit (Na_2SO_4:K_2SO_4:Fe_2O_3 = 1.5:1.5:1 mol.) which has commonly been used in fireside corrosion screening trials and is a mix that forms alkali-iron tri-sulphate (identified in many investigations as a cause of fireside corrosion) was used in these tests. The air-fired tests were carried out at temperatures of 600, 650 and 700 °C and oxy-fired tests were carried out at temperatures of 600, 650, 700 and 750 °C to represent the superheater/reheater metal temperatures anticipated in future power plants with and without synthetic deposits, with four candidate materials: T92, HR3C and 347HFG steels; nickel-based alloy 625 (alloy 625 was only tested with screening deposits). The progress of the samples during their exposures was measured using mass change methods. After the exposures, the samples were examined by SEM/EDX to characterise the damage. To quantify the metal damage, pre-exposure micrometre measurements were compared to the post-exposure image analyser measurements on sample cross-sections. The trends in corrosion damage in both air and oxy-firing conditions showed a "bell-shaped" curve, with the highest metal damage levels (peak) observed at 650 °C for air-firing and 700 °C for oxy-firing tests. However, at 600 and 650 °C similar damage levels were observed in both environments. The shift in peak corrosion damage in oxy-firing condition is believed to be the presence of higher levels of SOx, which stabilised the alkali-iron tri-sulphate compounds. Generally, in both air and oxy-firing conditions the mean metal damage was reduced with increasing the amount of Cr in the alloys. However, at the highest temperatures in both air-firing (700 °C) and oxy-firing conditions (750 °C) the metal damage of nickel based superalloy 625 was higher than HR3C.

© 2013 The Authors. Published by Elsevier Ltd. All rights reserved.

1. Introduction

Conventional fossil fuel fired power plants are believed to be significant contributors to the enhanced greenhouse effect/global warming [1,2]. CO_2 is one of the major greenhouse gases and various national, EU and international legislations are in place to reduce the CO_2 emissions from fossil fuel fired power plants. The UK government has an ambitious target of reducing CO_2 emissions to 80% of their 1990 levels by 2050 [2]. To meet this target a combination of renewable fuels such as biomass, which can be classed as carbon neutral, and carbon capture and storage (CCS) technologies such as oxy-fuel combustion will be necessary. A potentially carbon negative power generation is possible if co-firing of biomass and carbon capture technologies can be used together.

☆ This is an open-access article distributed under the terms of the Creative Commons Attribution-NonCommercial-No Derivative Works License, which permits non-commercial use, distribution, and reproduction in any medium, provided the original author and source are credited.

* Corresponding author. Tel.: +44 1234750111.
E-mail address: t.hussain@cranfield.ac.uk (T. Hussain).

0016-2361/$ - see front matter © 2013 The Authors. Published by Elsevier Ltd. All rights reserved.
http://dx.doi.org/10.1016/j.fuel.2013.04.005

Further reductions in CO_2 emissions from pulverised coal-fired power plants can be achieved by increasing the operating pressures and temperatures of their steam systems (which in turn increases the overall efficiency of the plants) [3], since each 1% increase in absolute efficiency results in as much as a 3% reduction in CO_2 emissions [4].

Co-firing low levels of biomass in conventional pulverised coal-fired power plants has proved to be a successful way to introduce carbon neutral biomass fuels into the electricity generation market to meet national and EU legislation. Biomass is a major contributor to renewable energy production, accounting for approximately 70% of worldwide renewable energy production [5]. Power plants burning biomass alone as fuel face significant issues with fouling, deposition, agglomeration and corrosion, which restricts the steam temperatures that can be used and so reduce the overall efficiency of the plants. However, these issues can be significantly reduced by the co-firing of biomass and coal [5–9]. The existing pulverised coal fired power plants are much larger in capacity and more efficient than dedicated biomass fired plants, so a few percentages of biomass co-fired with coal will provide more biomass derived renewable energy than a dedicated biomass plant using the same amount of biomass. Co-firing low levels of biomass can be achieved without making any major modifications (except fuel feeding and storage) to the existing coal-fired power plants.

Oxy-fuel firing is one of the possible routes for post-combustion capture where CO_2 is removed from the flue gas [1,8]. In oxy-fuel firing combustion is carried out in an O_2–CO_2–steam environment instead of air to produce a flue gas stream of minimal N_2 content and high CO_2 content which can be separated, compressed and stored in geological sites. Increased levels of CO_2 and H_2O coupled with higher levels of SO_2 and HCl (up to five times the levels of SOx found in conventional boilers using the same fuel, depending on the flue gas recycling configuration [1,8]) can lead to aggressive corrosion attack to the superheaters/reheaters. Oxy-fuel firing is expected to result in different gas chemistries and deposit compositions compared to conventional combustion systems.

Fireside corrosion (i.e., metal loss of heat exchangers due to chemical reactions with the combustion gases and deposits at high temperatures) has been a life-limiting factor for the pulverised fuel fired power plants. Fireside corrosion is one of the key reasons for tube failures in power plants. Fireside corrosion can lead to failure of superheaters/reheaters either by general metal loss or by the formation of cracks which can allow failure to occur by mechanical damage. Such failures are difficult to repair and results in unscheduled plant down time. In pulverised coal fired power plants molten alkali-iron tri-sulphates can form in the deposits on heat exchanger surfaces, which are very aggressive in nature [8,10]. However, when biomass is co-fired the combustion gases and deposits do not remain the same. Herbaceous biomass has higher levels of elements such as K and Cl but much less S compared to most coals [8,9,11,12]. Since the introduction of biomass, the issue of fireside corrosion has become more pronounced. Oxy-firing pulverised fuel power plants provides one potential route to enable post-combustion CO_2 capture, which in-turn requires higher temperature/pressure steam system to counter-act the energy required to run the CO_2 capture/compression units. Furthermore, the higher operating temperatures in future power plants will result in higher than acceptable metal damages for conventional superheater/reheater materials. In absence of preventative action, the increased steam system operating temperatures, co-firing of biomass and oxy-firing conditions will have a significant effect on the fireside corrosion of the heat exchanger materials; resulting in premature component failure and unscheduled shut-downs.

This paper reports the results of a comprehensive study of candidate superheater/reheater materials (a ferritic alloy: T92, two austenitic alloys: 347HFG and HR3C and a nickel based alloy: 625) in simulated air-fired and oxy-fired combustion gases (with hot gas recycling before flue gas de-sulphurisation) at metal temperatures higher than the average conventional temperatures (e.g., 540–560 °C [13,14]) of existing pulverised fuel power plants. The gas/deposit environments were selected based on co-firing a UK coal with cereal co-product. The performances of the alloys were investigated with/without a synthesis deposit to assess gas/deposit induced corrosion attack at 600–750 °C. This work was carried out using the "deposit recoat" technique that has been developed for high temperature corrosion [15–17]. Dimensional metrology has been used as the primary route to quantify the metal damage occurring due to fireside corrosion. After the exposures, the samples were examined by SEM with EDX mapping to characterise the damage. The data generated from these tests are now being used in an on-going programme that is developing models of fireside corrosion of superheater/reheater materials, as one element of life-time modelling of heat exchangers in advanced power generating systems [18].

2. Experimental methods

2.1. Materials

In this study, one ferritic steel (T92), two austentic steels (347 HFG, HR3C) and one nickel based alloy (625) were used to represent candidate materials for heat exchangers (supeheater/reheaters) in advanced pulverised fuel power plants. The nominal compositions of all four alloys are shown in Table 1. The materials were sourced as long tubes (i.e., boiler tubes) which were then cut and machined into tube segments with dimensions of ~15 mm chord, 15 mm long and 4 mm wall thickness. The surfaces of all the samples were prepared to a UK 600 grit surface finish.

2.2. Exposure conditions

The exposure conditions were determined following a detailed investigation of the gaseous environments and deposit conditions that could be found around superheater/reheaters in conventional pulverised coal fired UK plants using various biomass-coal fuel combinations [8,18]. The gaseous conditions for the fireside tests were based on co-firing 80:20 wt.% of a typical UK coal (Daw Mill) with cereal co-product (CCP). The compositions of these fuels are available in [19]. The gas compositions produced by these fuels in (a) air-firing and (b) oxy-firing (with hot gas-recycle following particulate removal but before flue gas de-sulphurisation) modes have been calculated from the fuel compositions, using models that have been validated through pilot and plant scale operations.

Table 1
Nominal composition of alloys used in fireside corrosion exposures (data in weight %).

Materials	Cr	Mo	Ni	Si	Mn	P	S	C	Fe	Others
T92	9.5	0.6		⩽0.5	⩽0.6	⩽0.02	⩽0.01	0.13	Bal.	0.25 V; 2 W; 0.09 Nb; 0.07 N
347 HFG	17–19		9–13	⩽0.5	⩽2	⩽0.045	⩽0.03	0.08	Bal.	0.6 < Nb + Ta < 1
HR3C	25		20	0.75	⩽2	⩽0.04	⩽0.04	0.1	Bal.	0.4 Nb; 0.2 N
Alloy 625	20–23	8–10	Bal.	⩽0.5	⩽0.5	⩽0.015	⩽0.015	.01	5	1 Co; 0.4 Al

Table 2
Nominal gas compositions used in fireside corrosion exposures.

	N_2 (vol.%)	O_2 (vol.%)	CO_2 (vol.%)	H_2O (vol.%)	SO_2 (vppm)	HCl (vppm)
Air-firing	73.8	4	14	8	1300	400
Oxy-firing	5.2	4	59	31	6260	1700

Table 3
Deposit compositions used in fireside corrosion exposures (composition in mole %).

	Na_2SO_4	K_2SO_4	Fe_2O_3
D0 (bare)	–	–	–
D1	37.5	37.5	25

These gas compositions have been simplified to their key active components for the purposes of corrosion testing in superheater/reheater environments. The nominal compositions of the gas in air-firing and oxy-firing conditions are given in Table 2. The alloys were tested at 600, 650 and 700 °C in air-firing condition and 600, 650, 700 and 750 °C in oxy-firing condition. All the alloys were tested both without any deposit (referred to as D0) and with a standard deposit (referred to as D1, with the composition give in Table 3). D1 is a widely used standard deposit for screening tests in fireside corrosion as it represents a composition of alkali-iron tri-sulphate that has been identified as being the principle cause of fireside corrosion on superheater/reheaters in pulverised coal fired stations [8,10,20–22].

2.3. Experimental setup

The fireside corrosion exposures were carried out in an alumina lined vertical controlled-atmosphere furnace using simulated air-fired combustion gases and simulated oxy-fired combustion gases. The furnace holds 24 test pieces at one time in alumina crucibles in the furnace hot zone. Pre-mixed gases were supplied to the controlled-atmosphere furnace through mass flows controllers to achieve the desired gas composition. A schematic diagram of the furnace set-up to simulate air-firing conditions is shown in Fig. 1 and a schematic diagram of the furnace set-up to simulate oxy-firing conditions is shown in Fig. 2. The key difference between the two test setups is the way water was introduced to the controlled atmosphere furnace. In the air-firing setup, the gas containing (CO_2, O_2, N_2) was passed through a de-ionised water bubbler which was kept at 40 °C in a water bath to add the required amount of moisture to the gas stream before mixing with the corrosive species (HCl, SO_2). In the oxy-firing setup, de-ionised water was directly injected to the furnace using a peristaltic pump, due to the higher level of moisture required. The furnace flange in oxy-firing setup was kept at 80 °C to stop condensation inside the furnace. The exhaust gases from the furnace passed through a condenser coil, an initially empty bottle to trap condensate and then through a scrubber solution (NaOH) before finally being vented into the atmosphere.

Each test was run for 1000 h using the widely accepted "deposit-recoat" method [15–17]. The samples were cleaned before exposure using a degreaser (volasil) followed by isopropanol (IPA) in an ultrasonic bath for 20 min. For the samples being exposed with a surface deposit (D1), the cleaned samples were painted using a paint brush to apply a deposit loading of ~20 mg/cm^2. The deposit (D1) was mixed with IPA to form thick slurries for painting onto the specimens. The tests were cycled every 200 h and repainted with deposits to replenish any salts, resulting in a deposition flux of ~100 μm/cm^2/h. The samples were weighted every 200 h with and without crucibles as well as before and after applying the deposits.

2.4. Pre and post-exposure measurements

Following exposure the samples were vacuum mounted using a low shrinkage cold mounting resin filled with ballotini (to further reduce shrinkage) in a specially designed jig. The mounted samples were then cross-sectioned, ground and polished to 1 μm diamond grit finish using non-aqueous lubricants. Environmental Scanning Electron Microscope (ESEM) was used to investigate the scale layer thicknesses and microstructures on the polished cross-sections. Energy dispersive X-ray (EDX) spectroscopy was used to identify the composition of the scales/deposits on the cross-sections. To identify the elemental distribution of key components across the scale/metal interfaces EDX mapping was used.

The dimensions of each of the samples were measured before and after the exposure. The dimensional metrology of the samples before and after exposure in the fireside corrosion tests is a key element of this research. All samples were measured using a digital micrometre (with resolution of 1 μm) prior to their exposure.

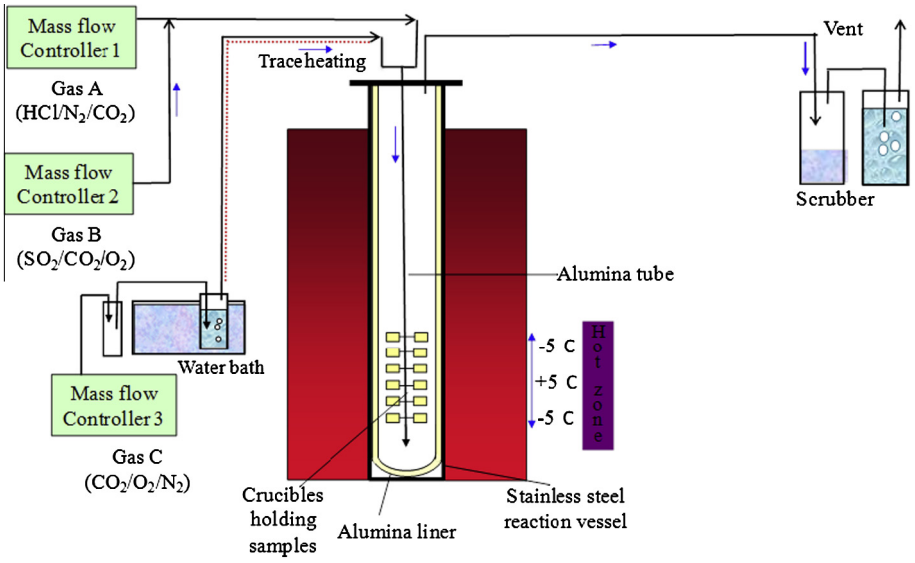

Fig. 1. Schematic diagram of a controlled atmosphere furnace setup for fireside corrosion in simulated air-firing combustion gases.

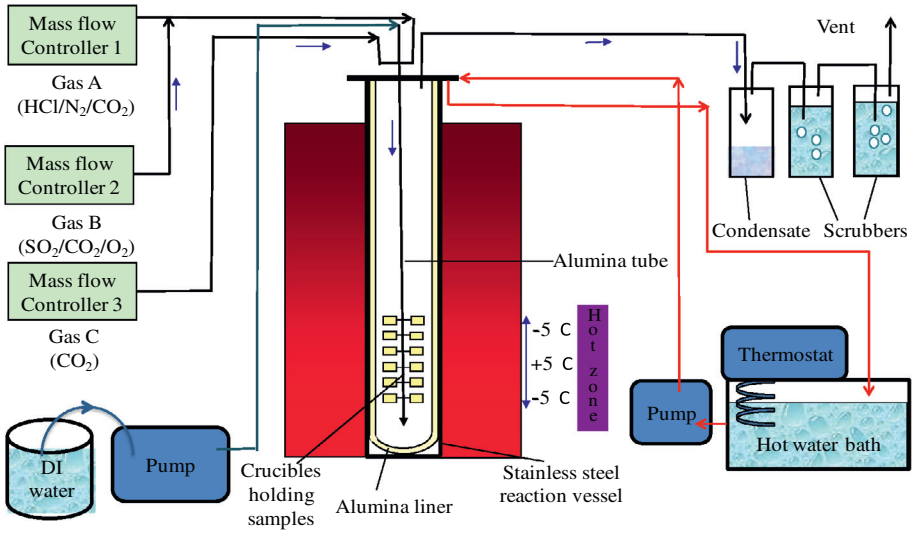

Fig. 2. Schematic diagram of a controlled atmosphere furnace setup for fireside corrosion in simulated oxy-firing combustion gases.

Post-exposure of sample cross-sections was carried out, using an image analyser connected to an optical microscope with a motorised *x–y* co-ordinate stage, to determine the remaining metal thickness and any internal damage. The measured co-ordinates from the post-exposure image analysis were transferred into spreadsheets and compared with the pre-exposure micrometre measurements to determine metal loss data distributions for each sample. These distributions were further processed to generate cumulative probability curves. A detailed description of the method is available in previously published papers (e.g. [19,23]). This measurement method was performed in accordance with the draft standard methods for high temperature corrosion assessments [15–17].

3. Results and discussions

3.1. Microstructural investigations

3.1.1. Effect of temperature on bare alloys

Back-Scattered Electron (BSE) images of the cross-sections of T92, 347 HFG and HR3C following 1000 h of exposure at 600, 650, and 700 °C in simulated air-fired combustion gases (1300 vppm SO_2, 400 vppm HCl) without any deposit (D0) are shown in Fig. 3. A thick multi-layered scale formed on T92 alloy, with voids within the scale, at all three temperatures. The scale formed at the lowest temperature (600 °C) is more compact than those from the other two temperatures. The scale at 650 °C shows buckling of the outer layer (due to stresses in the scale), which had resulted in its delamination from the inner layers that remain attached to the substrate. At 700 °C, the scale on T92 had completely delaminated from the substrate. The overall thickness of the scale increased on T92 from 600 °C to 650 °C, and reduced from 650 °C to 700 °C. As expected, the scales formed on austenitic alloys (347 HFG and HR3C) are much thinner than those formed on the lower Cr content ferritic alloy (T92) [24]. On 347HFG, the scales formed at 650 °C were thicker than those formed at either 600 or 700 °C; a similar trend was also observed in HR3C. Internal damage was observed in both the austenitic alloys, particularly at 650 °C. There was no sign of internal oxidation of T92 in the range of temperatures investigated in this study. Generally, the results show that much thicker scales were formed on T92, with progressively thinner scales being formed on 347 HFG and HR3C (with increasing chromium content). These results are in line with the expected trend in scale development for these alloys [25,26].

Fig. 4 shows the BSE images of the cross-sections of T92, 347 HFG and HR3C following exposure at 600, 650, 700 and 750 °C in simulated oxy-fired combustion gases (6260 vppm SO_2, 1700 vppm HCl) without any deposit (D0) after 1000 h. Similar to the air-firing conditions, the scales formed on T92 at all temperatures are thicker than those formed on 347 HFG and HR3C. However, the scales formed in simulated oxy-firing conditions are thicker than the scales formed on the corresponding alloys in air-fired conditions (i.e., at 600 °C the scale on T92 was 118 μm in oxy-fired compared to 86 μm in air-fired). The scale formed on T92 at 700 °C is much thicker than scales formed at any other temperatures (600, 650 and 750 °C). For both austenitic steels (347 HFG and HR3C) internal corrosion damage was observed in the temperature range of 650–750 °C. In both air-fired and oxy-fired combustion gases internal damage (inter-granular attack) was observed at the cross-sections of both austenitic steels $\geqslant$650 °C.

3.1.2. Effect of temperature on alloys covered with deposit

Fig. 5 shows the BSE images of cross-sections through T92, 347HFG, HR3C and alloy 625 samples that had been exposed covered in deposit D1 for 1000 h at 600, 650 and 700 °C in simulated air-fired combustion gases. Deposit D1 is considered to be an aggressive deposit which can form alkali-iron tri-sulphate in combination with the simulated combustion environment. Alkali-iron tri-sulphate has frequently been identified as the key component for superheater/reheater corrosion in pulverised coal fired power plants where the gaseous environment at the exposure temperatures generates sufficient SO_3 to stabilize the compound [22,24,27].

In all cases the scale/deposit layers are significantly thicker than those formed without any deposit (D0) (i.e., compared with Fig. 3). At both 600 and 650 °C, the microstructures of T92 show compact inner layers and porous outer layers, but a thicker band-like multi-layered structure at 700 °C. The scale/deposit layers formed on the austenitic alloys (347 HFG and HR3C) are also very thick with numerous voids and shows inter-layer delamination. At 600 °C HR3C showed the formation of relatively thin scale with good adhesion to the substrate; however, the scale/deposit layers were significantly thicker at 650 and 700 °C. At 600 °C the nickel-based alloy 625 showed scale/deposit layers, which were not apparent after exposure at 650 and 700 °C, possibly due to spallation or de-lamination during sample preparation.

BSE images of cross-sections through T92, 347HFG, HR3C and alloy 625 samples that had been exposed covered in deposit D1

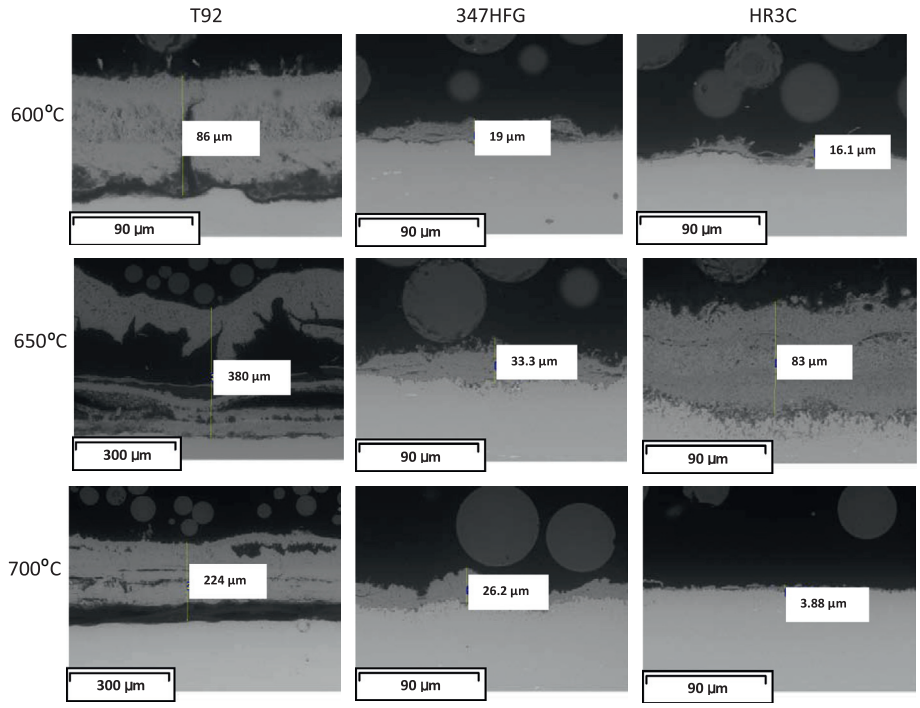

Fig. 3. BSE images of cross-sectioned scales on bare T92, 347HFG and HR3C exposed to simulated air-fired combustion gases (with 1300 vppm SO_2/400 vppm HCl) at 600, 650 and 700 °C for 1000 h.

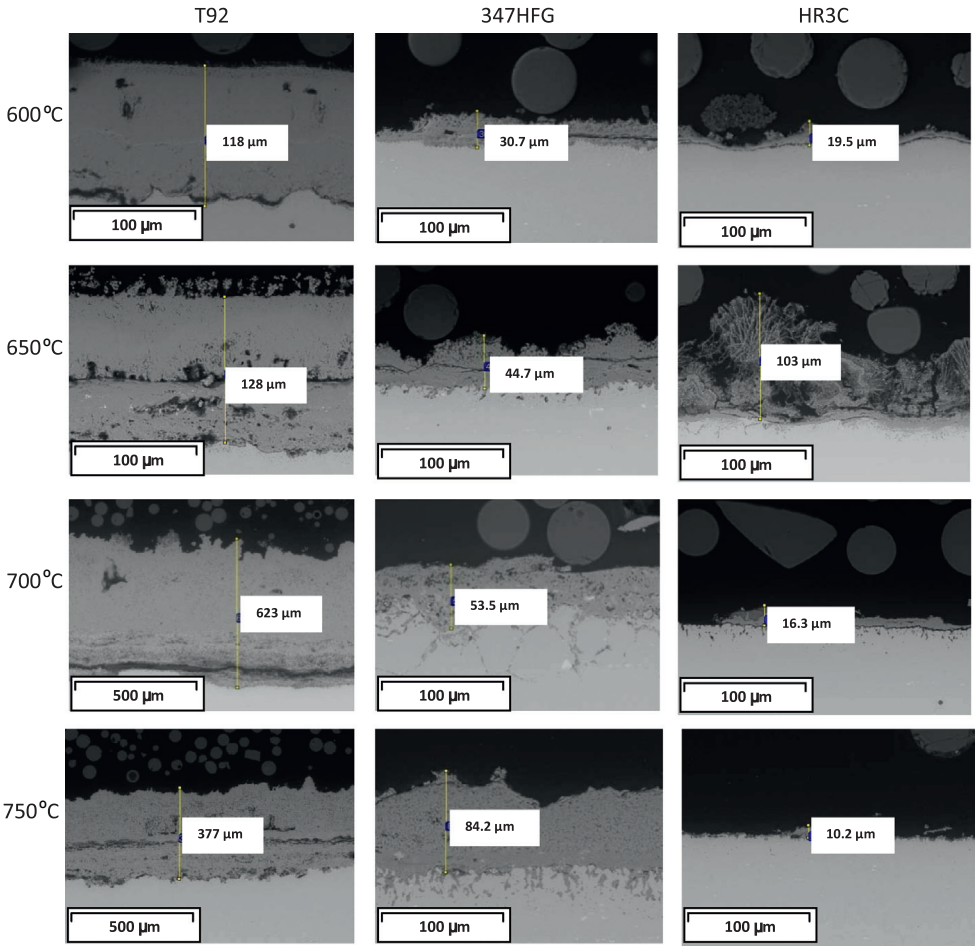

Fig. 4. BSE images of cross-sectioned scales on bare T92, 347HFG and HR3C exposed to simulated oxy-fired combustion gases (with 6260 vppm SO_2/1700 vppm HCl) at 600, 650 700 and 750 °C for 1000 h.

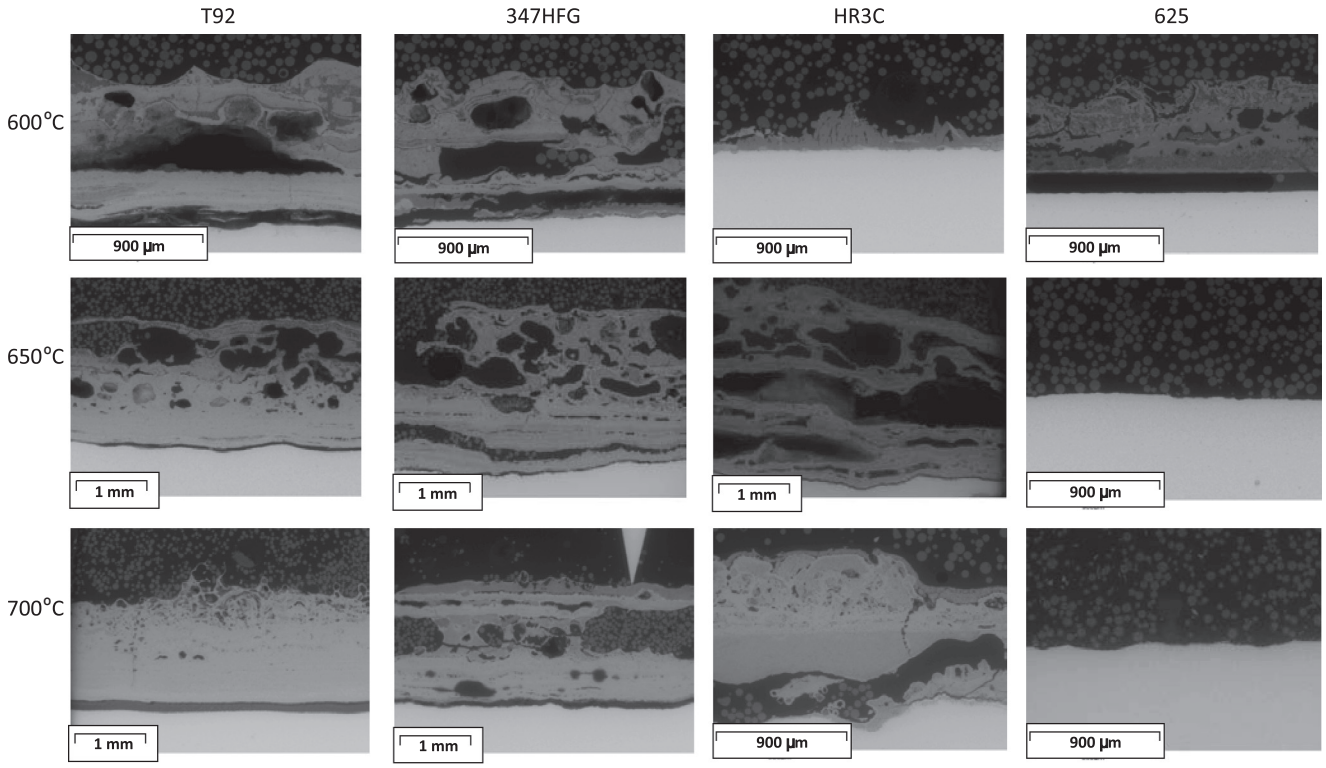

Fig. 5. BSE images of cross-sectioned scales on T92, 347HFG, HR3C and alloy 625 covered with deposit D1 exposed to simulated air-fired combustion gases at 600, 650 and 700 °C for 1000 h.

for 1000 h at 600, 650, 700 and 750 °C in simulated oxy-fired combustion gases are shown in Fig. 6. Similar to the samples from air-firing tests, the deposit/scale formed on T92 had a compact inner layer and a porous outer layer; however, the scale/deposit thickness is significantly greater in simulated oxy-firing test conditions (particularly at 700 °C). The thickest deposit/scale layer was formed on T92 at 700 °C (>1 mm thick). Similar to T92, the deposits/scale formed on 347 HFG, HR3C and alloy 625 appeared to be the thickest at 700 °C. 347HFG at 600 and 650 °C did not show any scale/deposit layer, probably due to spallation. Alloy 625 showed deposits/scale formation at all temperatures without any significant internal attack.

3.1.3. EDX mapping

EDX mapping was carried out on many sample cross-sections and as an example, EDX maps of T92 (without any deposit D0 and with deposit D1) exposed to simulated air-fired conditions at 650 °C for 1000 h are shown in Fig. 7. Fig. 7a shows the EDX maps without any deposit. In the maps oxygen and iron are distributed throughout the scale and the inner layer of the scale is enriched in chromium, suggesting the inner scale is composed of a spinel layer ($Fe_{(3-x)}Cr_{(x)}O_{(4)}$ where x is between 0 and 2) and the outer layer is a thick layer of magnetite (Fe_3O_4) with a thin haematite (Fe_2O_3) layer at the scale/gas boundary. Fig. 7b shows the EDX maps of cross section of T92 covered in deposit D1. Sulphur was found deep within the scale as elements from the deposits had infiltrated the scale during exposure. Chromium was enriched in the inner (spinel) oxide layer in a multi-layered arrangement and sodium and potassium (originally from the deposit) were found in increasing concentration towards the scale/gas boundary.

Fig. 8 shows the EDX maps of T92 exposed to simulated oxy-fired conditions (without any deposit D0 and with deposit D1) at 700 °C for 1000 h. The maps of the scale without any deposit (Fig. 8a) shows oxygen and iron distribution throughout the scale and enrichment of chromium in the inner layer, similar to the EDX maps of T92 exposed in the air-firing conditions. However, chromium is found in a multi-layered arrangement in the spinel layer rather than a thick band. The key difference in the EDX maps of the air-firing and oxy-firing conditions is in the quantity and the location of sulphur in the scale. Sulphur in oxy-firing environment successfully penetrated the scale and was seen at the metal/scale interface. Fig. 8b shows the maps of the scale with deposit D1 where molten deposits had infiltrated the scale during the exposure and a thick layer of sulphur was found at the metal/scale interface, similar to the air-firing conditions. Iron levels were depleted in the sulphur and chromium rich areas. Sulphur was detected beneath the chromium rich spinel layer. The role of sulphur in the corrosion mechanism can be confirmed by the detection of this sulphur rich layer at the inner scale.

3.2. Measurements of metal damage (dimensional metrology)

Dimensional metrology provides the most reliable measurement of the corrosion damage to alloys, as it produces a distribution of metal damage data for each exposed samples [15–18,28]. The results are plotted as "change in metal" or "metal- damage" as a function of cumulative probability according to the draft standards for high temperature corrosion measurements [15,16]. As an example Fig. 9 shows the "change in metal" versus cumulative probability for 347HFG covered with deposit D1 after exposure in the simulated oxy-fired combustion gases at 600, 650, 700 and 750 °C for 1000 h (note that a larger "change in metal" is more negative). The plot shows that the "change in metal" at 600 °C was the lowest of these four datasets, and that by increasing the test temperature to 650 °C and 700 °C the "change in metal" had increased (at 700 °C the "change in metal" had changed by 5–6

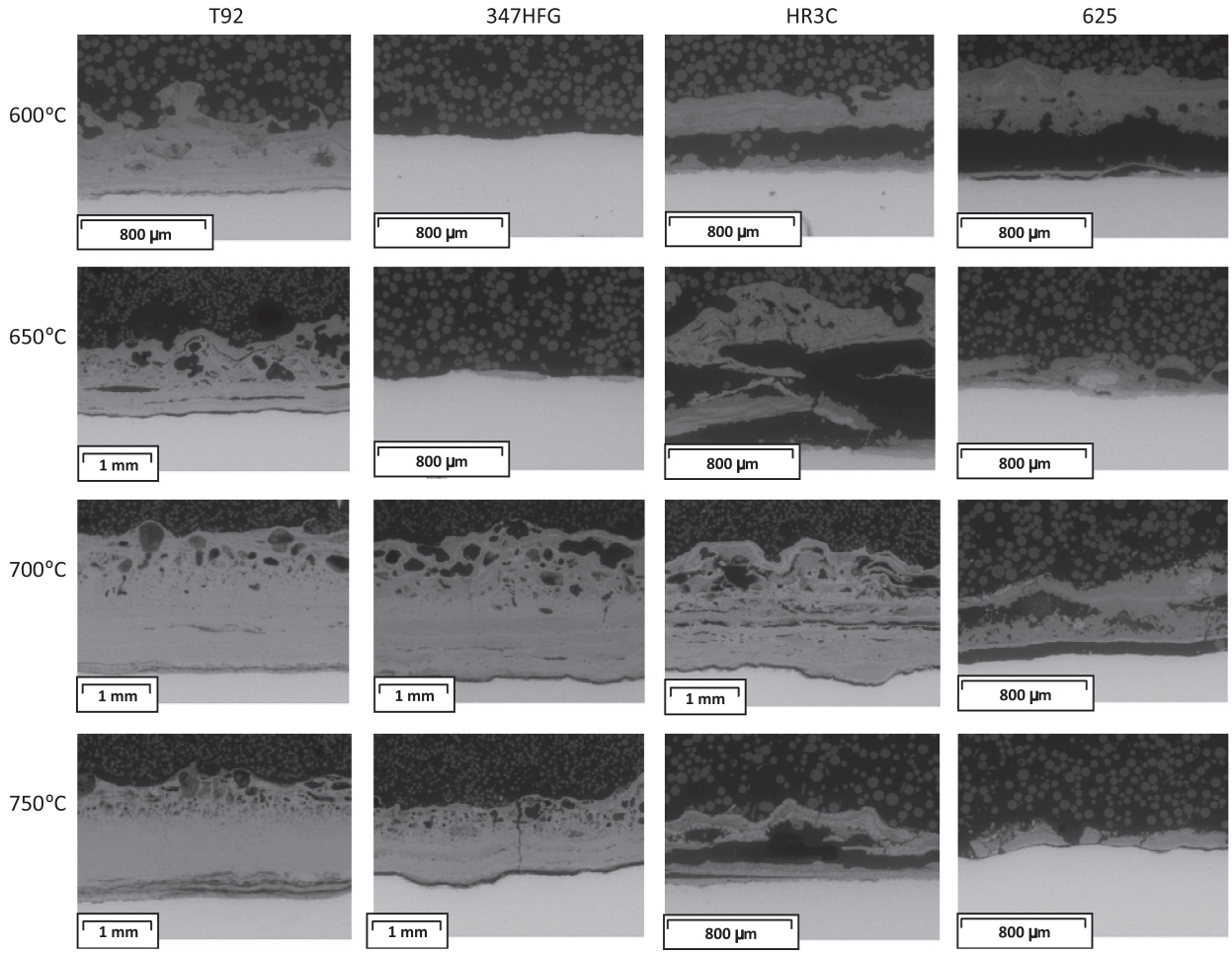

Fig. 6. BSE images of cross-sectioned scales on T92, 347HFG, HR3C and alloy 625 covered with deposit D1 exposed to simulated oxy-fired combustion gases (with 6260 vppm SO_2/1700 vppm HCl) at 600, 650 and 700 °C for 1000 h.

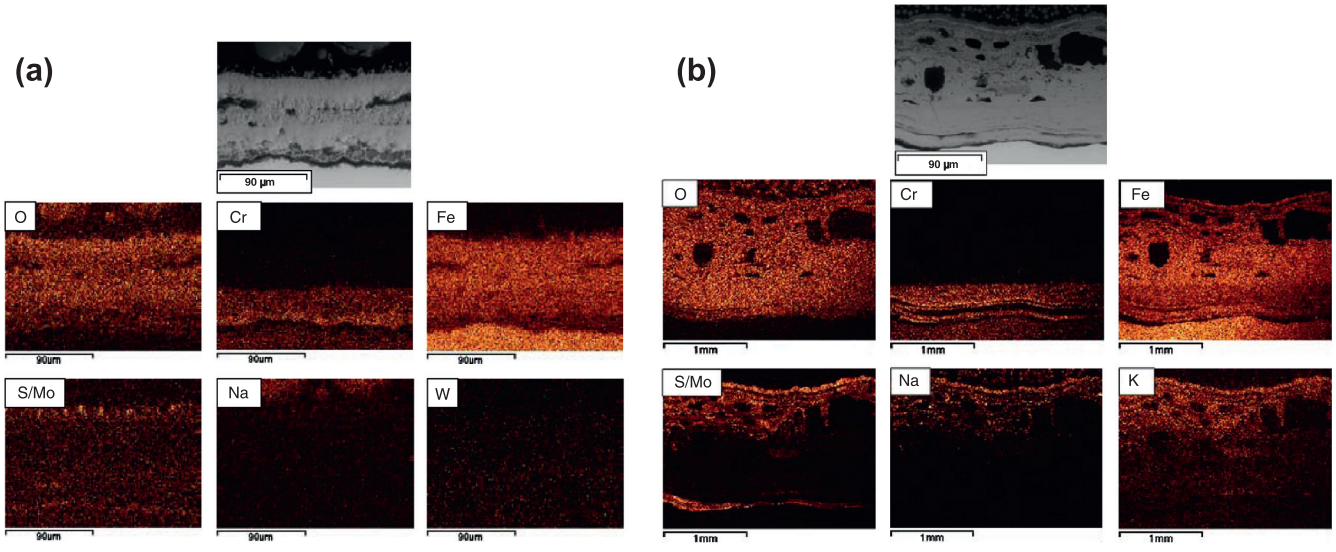

Fig. 7. BSE image and X-ray maps of cross-section through (a) bare T92 alloy and (b) covered in deposit D1 exposed to simulated air-fired combustion gases (with 1300 vppm SO_2/400 vppm HCl) at 650 °C for 1000 h.

times compared to the values at 600 °C). With further increase in the test temperature to 750 °C, the "change in metal" had decreased. This trend in "change in metal" data is in agreement with the scale thickness measurements and mass change measurements.

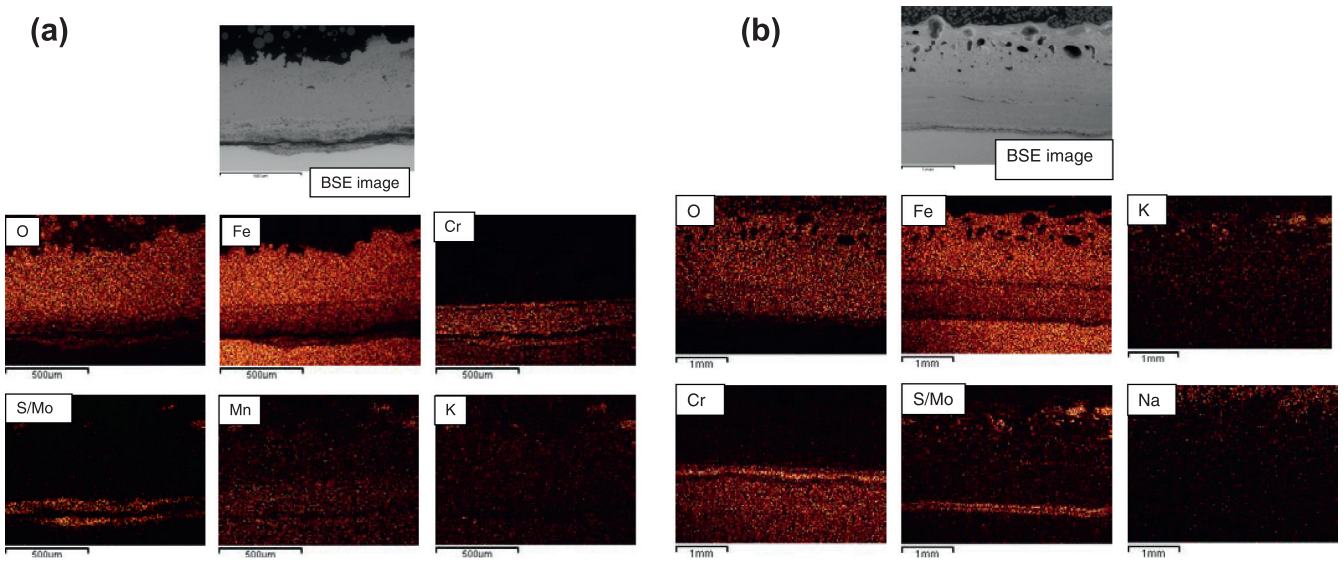

Fig. 8. BSE image and X-ray maps of cross-section through (a) bare T92 alloy and (b) covered in deposit D1 exposed to simulated oxy-fired combustion gases (with 6260 vppm SO_2/1700 vppm HCl) at 700 °C for 1000 h.

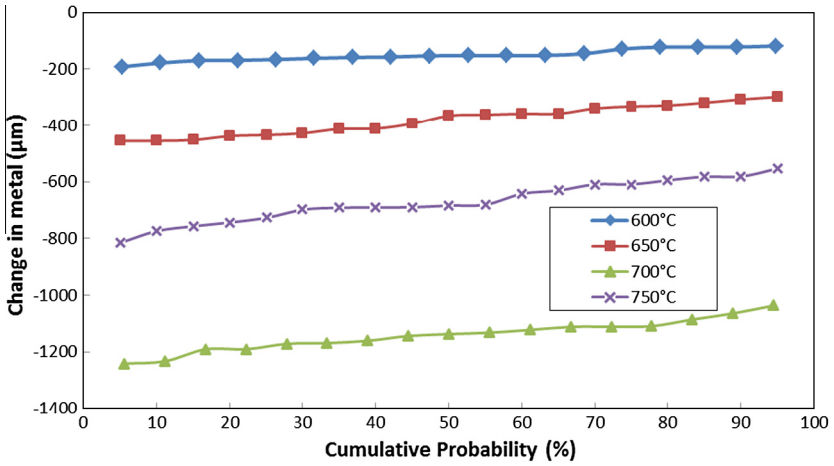

Fig. 9. Change in metal versus cumulative probability showing the behaviour of alloy 347HFG covered with deposit D1 after exposure in the simulated oxy-fired combustion gases at 600, 650, 700 and 750 °C for 1000 h.

3.2.1. Effect of temperature on bare alloys

The median "change in metal" values for all the alloys without any deposit (D0) exposed in simulated air-fired and simulated oxy-fired environments are shown in Fig. 10 with the maximum and minimum values as error bars. The "change in metal" has been multiplied by "−1" and presented as metal loss in this paper. In air-fired environment, the metal loss on T92 increased from 600 °C to 650 °C and subsequently decreased when the temperature was increased to 700 °C, showing a "bell-shaped" curve with a peak at 650 °C. Ferritic alloy (T92) showed a significantly higher damage compared to the two austenitic alloys (347HFG and HR3C) at all three temperatures. In mixed corrosive gases at lower temperatures materials suffer from a combined oxidation–sulphidation attack which moves towards oxidation alone at the higher temperature [21]. The reaction between SO_2 and O_2 at lower temperature favours SO_3 but at higher temperature SO_2 formation is favoured. The presence of SO_3 in the environment promotes mixed oxidation/sulphidation mechanism [10,22,24]. The rates of both mechanisms increase with temperature, but the mixed oxidation/sulphidation will be faster, thus the net effect will be to have a peak when crossing the mechanism boundary with increasing temperature.

The median metal loss values in simulated oxy-fired conditions without any deposit (D0) shows "bell-shaped" behaviour of T92 and 347HFG, similar to air-fired environment. However the location of the peak, where the metal loss is maximum, for both alloys had increased from 650 °C in air-fired environment to 700 °C in oxy-fired environment. In simulated oxy-firing environment there are five times more SOx than air-fired environment. This higher amount of SOx had shifted the balance of SO_2/SO_3 in the environment and the mixed oxidation/sulphidation mechanism region is extended further than the air-fired environment. In oxy-firing environment, the peak damage levels of T92 increased by a factor of ~2 compared to the air-firing environment. Similarly, with 347HFG the peak damage level increased by a factor of ~6 in the oxy-firing environment (from 20 µm to 120 µm). The higher levels of SO_2, HCl, CO_2 and steam in the oxy-firing environment can contribute to such an increase of peak damage levels. However,

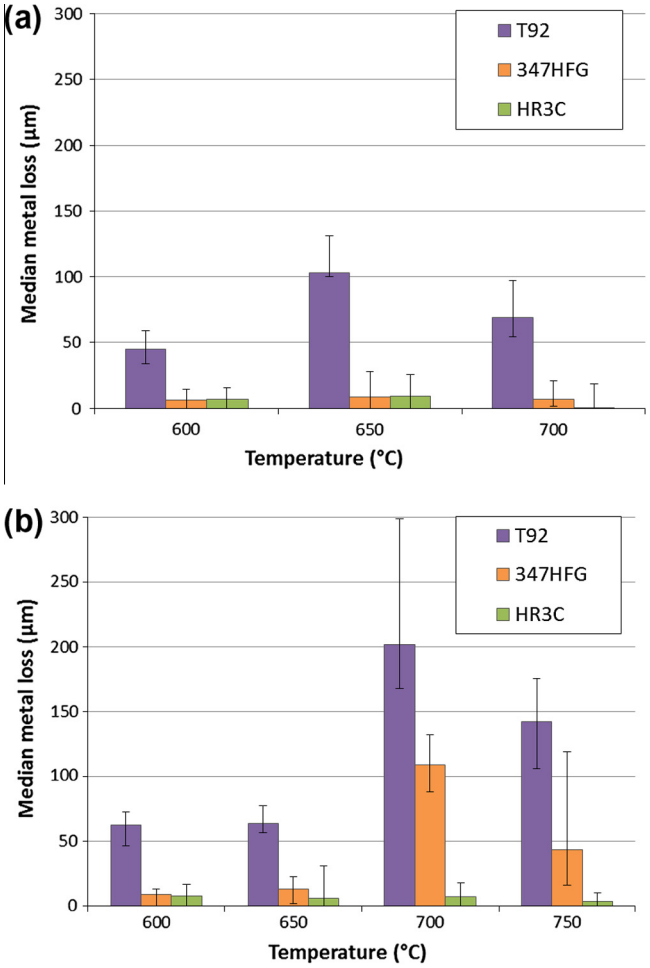

Fig. 10. Effect of temperature on median metal loss damage for bare alloys after 1000 h exposure in the (a) simulated air-fired combustion gases and (b) simulated oxy-fired combustion gases.

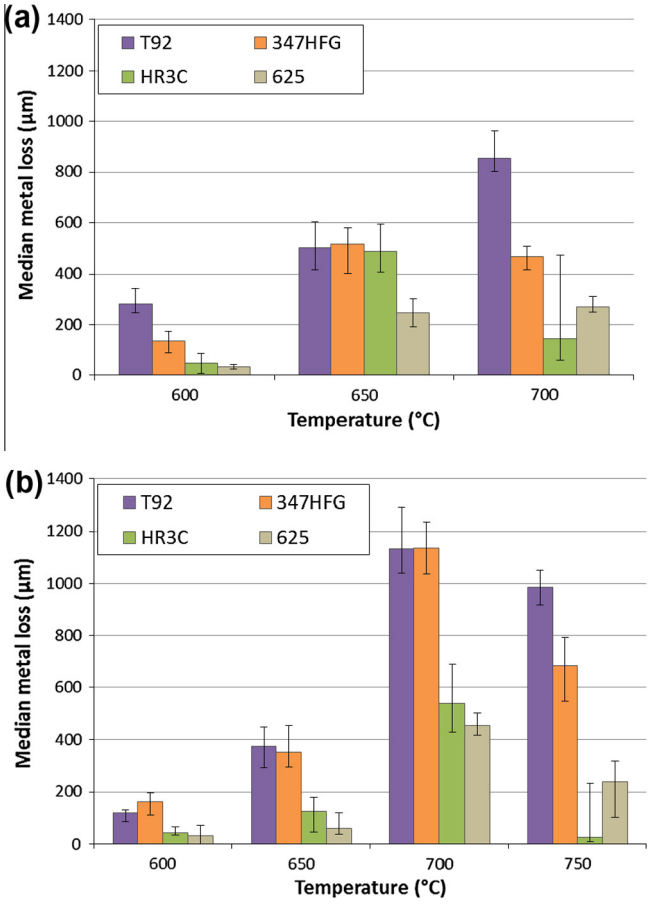

Fig. 11. Effect of temperature on median metal loss damage for alloys covered with deposit D1 after 1000 h exposure in the (a) simulated air-fired combustion gases and (b) simulated oxy-fired combustion gases.

at lower temperatures (600 and 650 °C) the median metal loss values for all three alloys were similar in both air-fired and oxy-fired combustion environments.

3.2.2. Effect of temperature on alloys covered with deposit

Fig. 11 shows the median metal loss for the alloys (T92, 347HFG, HR3C and 625) covered in deposit D1 in simulated air-fired combustion gases (Fig. 11a) and simulated oxy-fired combustion gases (for hot gas recycle option) (Fig. 11b). In both air-fired and oxy-fired conditions, all the alloys showed considerably more damage when covered with deposit D1 than only exposed to the gaseous environment (D0). Compared to the traditional target corrosion values for superheater/reheater materials in conventional power plants (~40–50 µm/1000 h [19]), the median metal loss values are excessive (it should be noted that D1 is an aggressive deposit that is used to accelerate superheater corrosion damage in laboratory exposures).

In general, the median metal damage for alloys had the following ranking (most to the least damage): T92 > 347HFG > HR3C. This can be explained by the levels of chromium present in the alloys. However, at 650 °C (at the peak corrosion damage) in simulated air-fired gases with deposits (D1), the metal losses for all three steels were very similar suggesting that even the 25 wt.% Cr in HR3C could not develop a more protective scale than the 9 wt.% Cr in T92 under this combination of exposure conditions. Similarly, in oxy-fired combustion conditions (hot gas recycle option) at 700 °C (at the peak corrosion damage) the median metal loss of T92 (9 wt.% Cr) was similar to 347HFG (18 wt.% Cr). At the highest test temperature in air-fired combustion environment (700 °C) and at the highest test temperature in the oxy-fired combustion environment (750 °C), nickel based alloy 625 was outperformed by the high chromium HR3C (25 wt.%). This suggests nickel based alloy 625 may have difficulties in developing protective layer with the more aggressive fireside corrosion conditions at high operating temperatures. It should be noted that HR3C contains more chromium than alloy 625 by 2–5 wt.%.

In these experiments with the candidate alloys covered with deposit D1, the highest metal losses were at 650 °C (except T92) in simulated air-fired conditions and at 700 °C in simulated oxy-fired combustion gases (for hot gas recycle option). This represents the characteristic "bell-shaped" curve for fireside corrosion damage which has been reported by many researchers e.g., [10,29]. The higher levels of SOx in the oxy-fired environment (0.63% compared to 0.13% in air-firing) contributed to the shift in the temperature at which maximum median metal losses were observed. The trends in median metal loss damages versus temperatures in both simulated air-fired and oxy-fired (hot gas recycle option) combustion gases covered with deposit D1 are shown in Fig. 12. The median metal loss values in simulated oxy-firing environments at 600 and 650 °C were lower than the values in conventional air-firing environments, suggesting oxy-firing (hot gas recycle option) may not be more aggressive than conventional air-firing conditions at those temperature ranges. The rate of increase of fireside corrosion damage for all four alloys from 600 to 650 °C in oxy-fired combus-

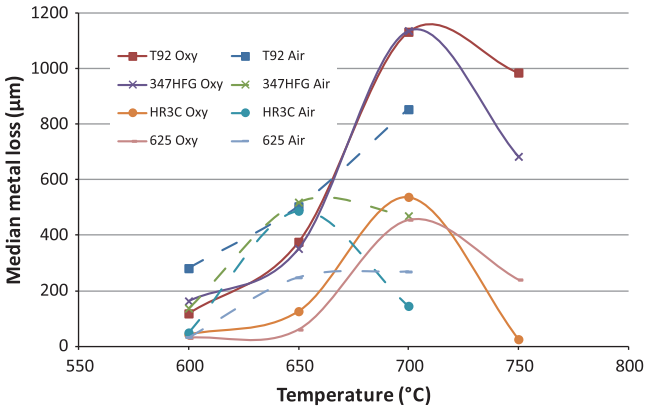

Fig. 12. Trends in median metal loss damage for alloys covered with deposit D1 after 1000 h exposure in the simulated air-fired and oxy-fired combustion gases.

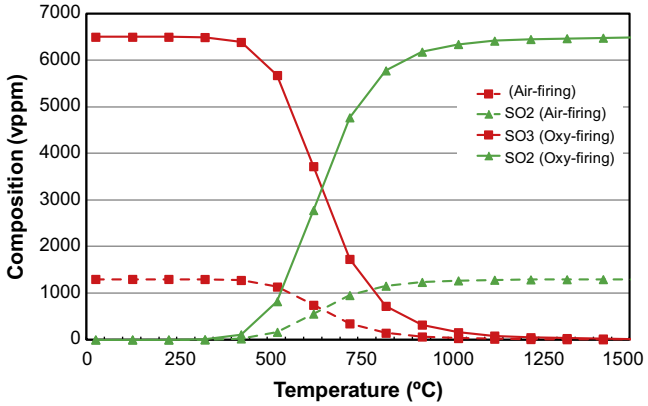

Fig. 13. Calculated compositions of SO_2 and SO_3 as a function of temperature using MTDATA in air and oxy-firing environments.

tion gases were also lower than the rates in air-fired combustion gases. The characteristic "bell-shaped" curve for fireside corrosion in oxy-firing combustion gases was shifted further to the upper-right hand corner – to higher temperatures and higher median metal loss values.

The peak in the corrosion rate is due to formation and de-stabilization of molten complex alkali-iron tri-sulphates with increasing temperature. Possible series of reactions of forming alkali-iron tri-sulphates are [30]

$$SO_2 + 1/2O_2 \leftrightarrow SO_3 \quad (1)$$

$$Fe_2O_3 + 3SO_3 \leftrightarrow Fe_2(SO_4)_3 \quad (2)$$

$$3(Na/K)_2SO_4 + Fe_2(SO_4)_3 \leftrightarrow 2(Na/K)_3Fe(SO_4)_3 \quad (3)$$

Alkali-iron tri-sulphates melt at a much lower temperature than alkali-sulphates, with a minimum melting point of ~550 °C compared to 832 °C [18,31–34]. Alkali-iron tri-sulphates need to be stabilized by SO_3. The alkali-iron tri-sulphates formed from the deposit D1 in the gaseous environment will have been molten at the exposure temperatures investigated. The rate of corrosion increases with increasing temperature in the presence of molten deposits (i.e., in the simulated air-fired conditions from 600 to 650 °C and in simulated oxy-fired conditions from 600 to 700 °C). However, the corrosion rate decreases as the deposit becomes unstable due to a shift in the balance of SO_2/SO_3 towards SO_2 at higher temperatures (i.e., in simulated air-fired combustion gases median metal losses decreased from 650 to 700 °C and in simulated oxy-fired combustion gases (with hot gas recycle) median metal losses decreased from 700 to 750 °C). The fireside corrosion rate has been reported to be at its highest between 650 and 680 °C by several researchers in conventional combustion environments [10,18,29,35]. Fig. 13 shows calculated compositions of SO_2 and SO_3 using thermodynamic modelling software MTDATA (NPL, UK) in both air and oxy-firing environments. As the temperature increases the levels of SO_3 decreases and the levels of SO_2 increases under thermodynamic equilibrium conditions- the shift in the balance of SO_2/SO_3 towards SO_2 occurs at around 725 °C.

4. Conclusions

The effect of simulated air-firing and oxy-firing combustion (hot gas recycle option) conditions on the fireside corrosion of the four different alloys: T92, 347HFG, HR3C and 625 has been investigated at 600–750 °C with and without a synthetic deposit for 1000 h. The "deposit-recoat" exposures were targeted at gaseous environment anticipated around superheaters/reheaters in future power plants operating in air-firing and oxy-firing (following particulate removal and before flue gas de-sulphurisation) conditions with a pulverized mix of 20 wt.% CCP with a typical UK coal. Dimensional metrology formed a critical part of this study which allows to quantify material damage and to produce metal loss distributions for statistical post-processing of data. The cross-sections of the samples were examined using ESEM/EDX.

Fireside corrosion damage to all the alloys in simulated oxy-fired combustion gas environments was similar to air-fired environments at 600 and 650 °C, but higher at 700 °C-due to a shift in peak corrosion damage. The corrosion damage for alloys exposed without deposit showed the highest corrosion damage at 650 °C in air-fired condition and at 700 °C in the oxy-fired condition. The shift in corrosion mechanism from mixed oxidation/sulphidation at lower temperatures to oxidation alone at higher temperatures is considered to be the reason. The trend in corrosion damage with temperature for all alloys covered with deposit D1 (generating alkali-iron tri-sulphates) in both firing conditions showed a "bell-shaped" curve, which is characteristic of superheater fireside corrosion damage, with the highest damage levels observed at 650 °C in air-fired conditions and 700 °C in oxy-fired conditions. The increase in peak corrosion damage in oxy-firing environment was due to the higher levels of SOx gases which stabilised the corrosion compounds (i.e., alkali-iron tri-sulphates). The decrease in the levels of metal damage at higher temperatures is due to the instability of the complex alkali-iron tri-sulphates, which requires SO_3 to stabilize. In both simulated air-firing and oxy-firing conditions, deposit D1 was found to damage all the alloys significantly more than just gaseous environment alone. Generally, the median metal damage for alloys had the following ranking (most to the least damage): T92 > 347HFG > HR3C > 625 (except at higher temperatures HR3C outperformed 625).

Acknowledgments

The authors acknowledge the support of The Energy Programme, which is a Research Councils UK cross council initiative led by EPSRC and contributed to by ESRC, NERC, BBSRC and STFC, and specifically the Supergen initiative (Grants GR/S86334/01 and EP/F029748) and the following companies; Alstom Power Ltd., Doosan Babcock, E.ON, National Physical Laboratory, Praxair Surface Technologies Ltd, QinetiQ, Rolls-Royce plc, RWE npower, Siemens Industrial Turbomachinery Ltd. and Tata Steel, for their valuable contributions to the project.

References

[1] Bordenet B. Influence of novel cycle concepts on the high-temperature corrosion of power plants. Mater Corros 2008;59:361–6.
[2] Skea J, Ekins P. Making the transition to a secure and low-carbon energy system. In: UKERC energy 2050 project; S3097:30; 2009.
[3] Natesan K, Park JH. Fireside and steamside corrosion of alloys for USC plants. Int J Hydrogen Energy 2007;32:3689–97.
[4] Henry J, Zhou G, Ward T. Lessons from the past: materials-related issues in an ultra-supercritical boiler at Eddystone plant. Mater High Temp 2007;24:249–58.
[5] Khan AA, de Jong W, Jansens PJ, Spliethoff H. Biomass combustion in fluidized bed boilers: potential problems and remedies. Fuel Process Technol 2009;90:21–50.
[6] Henderson P, Szakálos P, Pettersson R, Andersson C, Högberg J. Reducing superheater corrosion in wood-fired boilers. Mater Corros 2006;57:128–34.
[7] Montgomery M, Vilhelmsen T, Jensen SA. Potential high temperature corrosion problems due to co-firing of biomass and fossil fuels. Mater Corros 2008;59:783–93.
[8] Simms NJ, Kilgallon PJ, Oakey JE. Fireside issues in advanced power generation systems. Energy Mater: Mater Sci Eng Energy Syst 2007;2:154–60.
[9] Simms NJ, Kilgallon PJ, Oakley JE. Degradation of heat exchanger materials under biomass co-firing conditions. Mater High Temp 2007;24:333–42.
[10] Stringer J, Wright IG. Current limitations of high-temperature alloys in practical applications. Oxid Met 1995;44:265–308.
[11] Aho M, Gil A, Taipale R, Vainikka P, Vesala H. A pilot-scale fireside deposit study of co-firing Cynara with two coals in a fluidised bed. Fuel 2008;87:58–69.
[12] Nielsen HP, Baxter LL, Sclippab G, Morey C, Frandsen FJ, Dam-Johansen K. Deposition of potassium salts on heat transfer surfaces in straw-fired boilers: a pilot-scale study. Fuel 2000;79:131–9.
[13] Dechamps P. The EU research strategy towards zero emission fossil fuel power plants. In: Lecomte-Beckers J, Carton M, Schubert F, Ennis PJ, editors. Materials for advanced power engineering. Leige, Belgium: Grafische Medien; 2006. p. 25–40.
[14] Shingledecker JP, Wright IG. Evaluation of the materials technology required for a 760 °C power steam boiler. In: Lecomte-Beckers J, Carton M, Schubert F, Ennis PJ, editors. Materials for advanced power engineering. Leige, Belgium: Grafische Medien; 2006. p. 107–19.
[15] Draft code of practice for discontinuous corrosion testing in high temperature gaseous atmospheres. In: EC project SMT3-CT95-2001, TESTCORR. UK: ERA Technology; 2000.
[16] Corrosion of metals and alloys-methods for metallographic examination of samples after exposure to high temperature corrosive environments. In: Draft ISO Standard. ISO/TC 156 NWI 5092005; 2006.
[17] Saunders SRJ. Guidelines for methods of testing and research in high temperature corrosion. In: Grabke HJ, Meadowcroft DB, editors. London: The Institute of Metals; 1995. p. 85.
[18] Simms NJ, Fry AT. Modelling fireside corrosion of heat exchangers in co-fired pulverised fuel power systems. In: Lecomte-Beckers J, Carton M, editors. Materials for advanced power engineering. Julich: Forschungszentrum; 2010.
[19] Syed AU, Simms NJ, Oakey JE. Fireside corrosion of superheaters: effects of air and oxy-firing of coal and biomass. Fuel 2012;101:62–73.
[20] Raask E. Mineral impurities in coal combustion. Hemisphere Publishing Corporation; 1985.
[21] Natesan K, Purohit A, Rink DL. Coal-ash corrosion of alloys for combustion power plants. In: US department of energy fossil energy conference; 2003.
[22] Simms NJ. Environmental degradation of boiler components. In: Oakey JE, editor. Power plant life management and performance improvement. Woodhead Publishing; 2011. p. 145–79.
[23] Nicholls JR, Simms NJ, Encinas-Oropesa A. Modelling hot corrosion in industrial gas turbines. Mater High Temp 2007;24:149–92.
[24] Hussain T, Syed A, Simms N. Fireside corrosion of superheater materials in coal/biomass co-fired advanced power plants. Oxid Met 2013:1–12. http://dx.doi.org/10.1007/s11085-013-9394-y.
[25] Young D. High temperature oxidation and corrosion of metals. Elsevier; 2008.
[26] Birks N, Meier GH, Pettit FS. High-temperature oxidation of metals. Cambridge University Press; 2006.
[27] Srivastava S, Godiwalla K, Banerjee M. Fuel ash corrosion of boiler and superheater tubes. J Mater Sci 1997;32:835–49.
[28] Nicholls JR, Hancock P. Analysis of oxidation and hot corrosion data – a statistical approach. In: Rapp Robert A, editor. San Diego (CA, USA): NACE; 1983. p. 198–210.
[29] Reid W. External corrosion and deposits: boilers and gas turbines (Fuel and Energy Science). Elsevier Science Ltd.; 1971.
[30] Tomeczek J. Corrosion modelling of austenitic steel in molten sulphate deposit. Corros Sci 2007;49:1862–8.
[31] Hendry A, Lees DJ. Corrosion of austenitic steels in molten sulphate deposits. Corros Sci 1980;20:383–404.
[32] Cain CJ, Nelson W. Corrosion of superheaters and reheaters of pulverized-coal-fired boilers. II. Trans ASME 1961;83:468–74.
[33] Lindberg D, Backman R, Chartrand P. Thermodynamic evaluation and optimization of the ($NaCl + Na_2SO_4 + Na_2CO_3 + KCl + K_2SO_4 + K_2CO_3$) system. J Chem Thermodyn 2007;39:1001–21.
[34] Syed AU, Hussain T, Oakey JE, Simms NJ. Fireside corrosion of superheater materials in oxy-fired power plants. In: Eurocorr, Stockholm; 2011. p. 1062–78.
[35] Syed AU, Hussain T, Simms NJ, Oakey JE. Microscopy of fireside corrosion on superheater materials for oxy-fired pulverised fuel power plants. Mater High Temp 2012;29:219–28.